What ocean biogeochemical models can tell us about bottom-up control of ecosystem variability

Journal:	*ICES Journal of Marine Science*
Manuscript ID:	ICESJMS-2010-160
Manuscript Types:	Symposium Article
Date Submitted by the Author:	16-Jun-2010
Complete List of Authors:	Gnanadesikan, Anand; NOAA Geophysical Fluid Dynamics Lab, Oceans and Climate Group Dunne, John; NOAA Geophysical Fluid Dynamics Lab, Climate and Ecosystems Group John, Jasmin; NOAA Geophysical Fluid Dynamics Lab, C; NOAA Geophysical Fluid Dynamics Lab, Climate and Ecosystems Group
Keyword:	biome extent, climate models, nutrient limitation, salinity, size structure, spring bloom

What ocean biogeochemical models can tell us about bottom-up control of ecosystem variability

Anand Gnanadesikan, John P. Dunne and Jasmin John

Processes included in earth system models can amplify the impact of climate variability on phytoplankton biomass in ways that can affect upper trophic levels. Models predict much larger relative interannual variability in large phytoplankton biomass compared with total phytoplankton biomass, supporting the goal of better constraining size-structured primary production and biomass from remote sensing. The largest modeled variability in annually-averaged large phytoplankton biomass is associated with changes in the areal extent of relatively productive regions. Near the equator, such changes in areal extent of the high-productivity zone are driven by large scale shifts in nutrient fields and not just changes in circulation. Finally, models show that high-latitude interannual variability in large phytoplankton biomass is much higher during the spring. Mechanisms for producing shifts in spring bloom timing differ across biomes, complicating efforts to link ecosystem variability to climate modes defined using sea surface temperature. In salinity-stratified subpolar regions, changes in bloom timing driven by salinity can produce correlations between low surface temperatures and high productivity, supporting the potential importance of coupled reanalyses for attributing past ecosystem shifts.

Keywords: Biome extent, climate models, nutrient limitation, salinity, size structure, spring bloom

Anand Gnanadesikan, John P. Dunne and Jasmin John, NOAA Geophysical Fluid Dynamics Laboratory, 201 Forrestal Road, Princeton University, Princeton, NJ 08540 USA

P: 1-609-987-5062 E: anand.gnanadesikan@noaa.gov

Introduction

One of the most surprising interpretations of satellite ocean color data is the relatively low interannual variability of primary productivity. Estimates from the SeaWiFS satellite, using the algorithm of Carr (2001), show that on basin scales the primary productivity varies relatively little from year to year over the SeaWiFS period. Over the latitude band of 0-30N in the Pacific (black lines Figure 1a), the annual production varies by less than 1 mmol C/m^2/day out of an annual average of ~40. The region from 30N to 65N, as a whole (red lines, Figure 1a) also shows relatively little interannual variation. As seen in Figure 1b, coastal regions do show much more absolute variability, with the standard deviation of annually averaged primary production exceeding 20 mmol C/m^2/day over much of the Pacific margins. Yet these regions are also regions of relatively high productivity, so that when the interannual variation is divided by the mean (Figure 1c) the dominant signal is seen not in these highly productive regions, but rather along the edges of the subtropical gyres. A similar spatial pattern of variability also appears to hold on interdecadal time scales, as shown by a recent comparison (Martinez et al., 2009) between the Coastal Zone Color Scanner satellite era (1979-1983) and the first 5 years of the SeaWiFS satellite era (1998-2003) illustrated in Figure 1d.

Naïvely, this low variability in annually averaged primary productivity would appear to clash with high variability in the stocks of a number of species that has been reported on interannual to decadal scales and linked to climate modes such as the Pacific Decadal Oscillation and North Atlantic Oscillation. For example, basin scale modes in the Pacific have been linked to variability in such species as salmon in the Pacific Northwest (Mantua et al., 1997), walleye pollock in the Bering Sea (Hunt et al., 2002), Japanese eel in the Kuroshio region (Sugimoto et

al., 2001) and sardine and anchovy in the Peru Current (Chavez et al., 2003). Mechanisms proposed to explain such variability have included temperature impacts on spawning times and locations (e.g. Genner et al., 2004), changes in the frequency of warm events such as those associated with coral bleaching (Glynn and DeWeerdt, 1991), changes in the frequency of cold events associated with wintertime mortality (Hare et al. 2009), or changes in the advective pathways for larval transport (e.g. Sugimoto et al. 2001).

While not deprecating the potential importance of such direct physical forcing for individual species, this paper focuses on what can be learned from a more fine-grained examination of primary productivity. For many years, fisheries oceanographers have recognized that the details of primary production such as the timing of blooms (Hjort, 1914; Cushing, 1990) or differences in phytoplankton community structure (Ryther, 1969) could explain variations in ecosystems over time and space. We examine whether the large-scale Earth System Models used for projecting climate change represent such aspects of the primary productivity signal that both observations and theory suggest vary significantly from year to year. Additionally, we investigate what models can tell us about the magnitude of such variability and about the physical processes underlying it. We show that the current generation of Earth System Models do simulate drivers of interannual ecosystem variability beyond annually averaged changes in biomass. These drivers include changes in the areal extent of productive regions, changes in the timing of blooms and changes in the concentration of large phytoplankton.

Variability in the abundance of large phytoplankton is especially important, as their grazers have long been thought to represent the key pathway by which energy is transferred to higher trophic levels, leading to the classic statement that “all fish is diatoms” (Bigelow, 1926). In upwelling regions rich in macronutrients, larger phytoplankton dominate and recycling of

nutrient is inefficient (Dugdale and Goering, 1968). In weakly productive subtropical gyres where macronutrients are at low levels, small picoplankton have been found to account for most of the primary productivity (Platt et al., 1983) and recycling of nutrients is high. This leads to less variation in total biomass across biomes than would be expected from the differences in nutrient supply, as well as less spatial variability in small phytoplankton biomass than large phytoplankton biomass. Agawin et al. (2000) noted that the concentration of large plankton showed 5-6 orders of magnitude variation in mesocosm experiments, while small plankton biomass concentrations varied over about 2 orders of magnitude. Similar results for remotely sensed concentrations of large and small particle concentrations were recently presented by Kostadinov et al. (2009). The idea that such differences in size structure of primary producers, translated up the food web, are responsible for the differences in fisheries production between ecosystems goes back at least to Ryther (1969). However, since time series of size-fractionated productivity and biomass do not exist in most of the regions where large relative variability is seen, it is worth examining whether models can be used to characterize the variability of large phytoplankton on global scales.

The current generation of ocean biogeochemical and earth system models combine information about physical forcing, chemical cycling, phytoplankton physiology and ecological structure to simulate the response of lower trophic levels to climate variability and change (Six and Meier-Reimer, 1996; Moore and Doney, 2004; Aumont and Bopp, 2006; Galbraith et al., 2010). Built around ocean circulation models that use the conservation of heat, mass, salt and momentum to solve for a physical circulation consistent with surface forcing, such models can be forced by datasets based on atmospheric reanalysis products (Griffies et al., 2009) to produce retrospective estimates of biological activity. Alternatively, they can be embedded in fully

coupled ocean-atmosphere circulation models to estimate how ocean ecosystems could change in the future as a result of changes in greenhouse gasses (e.g. Steinacher et al., 2010).

This paper examines what such models can tell us about the potential for quantitatively and mechanistically linking variability in primary productivity to climate variability and change. Section 2 describes how the Tracers of Ocean Productivity with Allometric Zooplankon (TOPAZ) model used in the NOAA Geophysical Fluid Dynamics Laboratory's Earth System Model (Dunne et al., 2010) represents key ideas about phytoplankton size structure and describes two physical circulation models in which it has been implemented. Section 3 shows output from these simulations, quantifying the dominance of large phytoplankton variability over much of the ocean, further highlighting the importance of changes in areal extent of biomes, and also considering the impact of interannual variability in bloom timing. Section 4 expands on the mechanisms by which tropical variability on interannual time scales changes the areal extent of the oligotrophic tropical gyres. Section 5 expands on the mechanisms driving interannual variability in springtime productivity in four North Pacific regions. Section 6 concludes the paper by examining the implications of our results for observational strategies in characterizing fisheries and for developing new retrospective modeling analyses.

2. The models

a.) Size structure in the GFDL ecosystem models

We begin by examining how the Geophysical Fluid Dynamics Lab's TOPAZ code (Dunne et al., 2010) deals with the response of phytoplankton biomass to varying environmental conditions and how this differs between large and small phytoplankton. Like other

biogeochemical models of intermediate complexity, TOPAZ divides the phytoplankton community into a small number of functional groups which react differently to light and nutrient limitation. Nutrient-uptake limitation is parameterized in terms of the classic Michaelis-Menten curve

$$Lim_N = \frac{N}{K_N + N} \quad (1)$$

Where Lim_N denotes the limitation of uptake rate due to nutrient N, and K_N is a half-saturation constant for that nutrient. Light limitation is parameterized in terms of

$$Lim_{Irr} = 1 - \exp(-\alpha\theta I / P_N^C) \quad (2)$$

Where α is a photosynthetic efficiency term, θ is a chlorophyll to carbon ratio, I is the incoming solar radiation and P_N^C is the nutrient-limited carbon assimilation rate. The carbon to chlorophyll ratio changes so as to "match" the light harvesting capacity $\alpha\theta I$ with the growth rate P_N^C so that high levels of light or low levels of growth lead to lower chl:C ratios (Geider et al., 1997 as discussed in Galbraith et al., 2010 and Dunne et al., 2010),. Physiological nutrient limitation is determined from the actual N:P and Fe:P cellular quotas which change through a complicated process described in detail in Dunne et al. (2010) based on the theoretical work of Klausmeier et al. (2004). A key point is that nutrient limitation is determined by the minimum limiting nutrient.

TOPAZ distinguishes between three functional groups.

1. Small plankton: Meant to represent nanoplankton such as Synechecoccus and prochlorococcus, this class of phytoplankton has relatively low half-saturation coefficients for iron (5 nM), ammonia (0.2 μM), phosphorus (0.2 μM) and nitrate (2.0 μM).

2. Diazotrophs: Meant to represent organisms such as Trichodesmium which fix nitrogen from N_2, these organisms require four times as much iron as the small plankton and have a maximum growth rate 40% of the small plankton.

3. Large plankton: Meant to represent green algae, diatoms and other large phytoplankton, this class of plankton has half-saturation constants for uptake that are three times that for small phytoplankton, 33% higher maximum growth rates than small phytoplankton, and the ability to store iron internally. One obvious implication of these differences is that different phytoplankton will respond differently to nutrient availability. For example, changing nitrate from 2.0 μM to 4.0 μM will have a large impact of the extent to which large phytoplankton are nitrate-limited, but a relatively small impact on how small plankton are nitrate-limited.

Size has an additional impact on plankton concentration in TOPAZ in that it also governs the grazing of phytoplankton. Based on the work of Dunne et al. (2005) the equation governing a given class of phytoplankton biomass is

$$\frac{\partial P}{\partial t} = \mu_P P - \lambda \left(\frac{P}{P_*} \right)^a P \qquad (3)$$

where P is the concentration of some class of phytoplankton, μ_P is a growth rate, λ is a grazing rate, P_* is a scale concentration for grazing and a is the grazing parameter (a=1 for classic logistic growth). Dunne et al. (2005) then proposed that for small phytoplankton, which are grazed by zooplankton with a similar generation time, a=1. By contrast, for large phytoplankton a=1/3, so that the concentration of larger zooplankton varies much less than the concentration of their prey. If we replace P in (3) with S for small plankton and L for large plankton, the resulting steady-state concentrations are

$$S = \left(\frac{\mu_S}{\lambda}\right) P_* \qquad L = \left(\frac{\mu_L}{\lambda}\right)^3 P_* \tag{4}$$

Thus large phytoplankton concentrations will respond much more to changes in growth rate than will small phytoplankton concentrations. Sections 3 and 5 examine the magnitude of the changes in biomass produced by these changes in growth rate and link them to environmental drivers.

b.) Ocean-ice model

The ocean-ice model used in these simulations is the ocean-ice component of the GFDL CM2.1 global coupled climate model (Delworth et al., 2006). The model is configured with 50 vertical layers with thicknesses ranging from 10m over the top 200m to a maximum thickness of 250m at 5500m depth. The meridional resolution is 1 degree while the zonal resolution varies from 1 degree in mid-latitudes to 1/3 degree at the equator. North of 65 degrees a tripolar grid is employed to avoid the polar singularity. Up-to-date parameterizations of mixed layer dynamics, isopycnal mixing, advection by subgridscale eddies, bottom topography and bottom flows and lateral viscosity are included (Griffies et al., 2005; Gnanadesikan et al. 2006). Both the dynamics and thermodynamics of five thickness classes of sea ice are simulated.

Surface forcing is set using the Coordinated Ocean-ice Reference Experiment (CORE) protocol (Griffies et al., 2009) in which the inputs for calculating surface fluxes are taken from an atmospheric reanalysis data set adjusted so as to better agree with in-situ measurements. Sensible and latent heat fluxes are then calculated using bulk formulae. We will refer to these simulations as the CORE runs. In CORE forced models, freshwater forcing is given by a combination of applied precipitation, evaporation computed using bulk fluxes, and a correction diagnosed so as to restore surface salinities in the top 10m to climatological monthly values over

60 days. Without this correction, many models fail to maintain a robust Atlantic Meridional Overturning circulation (see section 16 of Griffies et al., 2009 for further discussion). However, the presence of such a correction damps long-period variability in salinity, with implications for biogeoechemical cycles. The resulting difficulty in simulating long-term salinity variability forms an important part of our motivation for examining coupled climate models.

c.) Coupled climate model

In coupled climate models, the incoming solar radiation, atmospheric greenhouse gases and aerosols, and some aspects of the land surface are fixed, but the air-sea fluxes of heat and momentum are then allowed to evolve freely. Such models can simulate the mean climate, its forced response to changes in the radiation balance and its intrinsic variability, but will not simulate the response of climate in any given year. One should thus look to the coupled models to match statistical relationships between biological features and physical forcing, not to simulate individual years or decades.

The model used for these runs is the Geophysical Fluid Dynamics Laboratory's Earth System Model 2.1 (ESM2.1). The physical core of this model is the CM2.1 global coupled climate model described in Delworth et al. (2006), with the baseline ocean solution described in Gnanadesikan et al. (2006). CM2.1 has an atmospheric physical climate that compares well against other global climate models (Reichler and Kim, 2008), an ocean circulation in the Southern Ocean that is quite realistic (Russell, Stouffer and Dixon, 2006) and a relatively realistic ENSO (Wittenberg et al., 2006; van Oldenborgh et al., 2005). Output is taken from

years 401-500 of a spinup with radiatively-active trace gasses fixed at 1860 levels, and thus should reflect the background level of unforced, internal variability in the climate system.

d.) Evaluation of model fidelity

The best characterized fields with which the models can be compared are the surface distribution of macronutrients. As shown by the red line in Figure 2a, the CORE ocean-ice model captures the large-scale distribution of phosphate, with higher values along the equator, higher values in the northern subpolar gyres and the highest values in the Southern Ocean. The model captures the tendency towards nitrate limitation that allows for unutilized phosphate in the subtropical gyres (nitrate, not shown, goes to essentially zero in the subtropical gyres). The model underestimates phosphate concentrations in the northern oceans. These basic patterns carry over to ESM2.1 (blue line,Figure 2a) where they are somewhat more pronounced.

Additional constraints on the model can be gleaned by comparing with products inferred from satellite remote sensing. The zonal integral of chlorophyll (Figure 2b), which is very similar between the ocean-only and coupled models, tends to underestimate the total chlorophyll inventory in part due to a failure to capture very high values in upwelling zones. The chlorophyll signal shows that low simulated surface nutrients in high northern latitudes are not due to an excess of productivity, suggesting that insufficient nutrient supply may be responsible. Zonal-mean primary productivity compares well with that estimated from SeaWiFS chlorophyll using the Carr, (2002) algorithm, (Figure 2c) in both the ocean-only and coupled models, with the differences between the models and observational estimates considerably smaller than differences between individual observational estimates (Gnanadesikan et al., 2004). The model

also captures the difference in ranges of large and small biomass (Figure 2d). Comparing monthly-mean values between 60N and 60S, we see that the small biomass ranges over about a factor of 20, while large biomass ranges over more than three orders of magnitude.

3. Results: Size structure and the disproportionate variability of large phytoplankton

We begin by examining the relative interannual variability (standard deviation/mean, also known as the coefficient of variability) of chlorophyll (Figure 3a) and primary productivity (Figure 3b) over a 46-year repeat cycle in the CORE run. Comparing Figure 3b to Figure 1c, we see that the relative variability is highest in both models and data at the edge of highly productive regions, particularly along the edges of the equatorial cold tongue and in upwelling zones. Relative interannual variability in productivity (Figure 3b) is generally smaller in amplitude than chlorophyll, though it is reasonably well correlated with it. As shown by the regression coefficient in the lower right of Figure 3b, a 10% change in chlorophyll would only be expected to produce a 5.2% change in productivity. A similar reduction is also seen in algorithms for computing primary productivity from satellite-estimated chlorophyll, as higher chlorophyll leads to higher light-harvesting capacity but also less penetration of solar radiation.

As might be expected from Figure 2d, the models predict very different variability for the biomass of large and small phytoplankton. Over most of the ocean, the relative standard deviation of small phytoplankton biomass (Fig 3c) is less than 10%, much smaller than for total chlorophyll. The pattern of chlorophyll variability is correlated with the changes in small biomass, with a correlation coefficient of 0.58 in the CORE run. However, a 10% change in chlorophyll only results in a 1.8% change in small plankton biomass. By contrast, the relative

variability in large plankton biomass (Figure 3d) is comparable to (and in some cases much larger than) the relative variability in chlorophyll. The bulk of the variability in productivity is thus in the large phytoplankton, not the small- even though small plankton make up the majority of the global phytoplankton biomass. The coupled model (not shown), shows similar patterns of variability as the CORE-forced simulation with much more variability in large phytoplankton, similar correlation and regression coefficients between chlorophyll and other fields, and the largest-amplitude variability occurring at the edge of the subtropical gyres and coastal upwelling regions.

Comparing the zonal average of the relative interannual variability (Figure 4a) further emphasizes the difference between small and large phytoplankton. The standard deviation of the total biomass (solid lines) is on average less than 10% of the mean over almost the entire ocean in both the ocean-only and coupled models. By constrast, for large biomass over the tropics a relative standard deviation of 35% is seen in both models.

Variability in the annual productivity is not, however, the only possible way in which biogeochemical variability can project into interannual changes in ecosystems. The "match-mismatch" hypothesis of Cushing (1990) builds on the classic work of Hjort (1914), suggesting that changes in the timing of spring bloom are more important than changes in the magnitude of productivity. This suggests analyzing the interannual variability in productivity month by month, with a particular focus on the spring bloom. Figure 4b shows the relative interannual variability in productivity for the month of April, a month for which the largest interannual variability was found. The biggest signal is the change in relative variability in high northern latitudes, with both total plankton biomass and large plankton biomass showing an increase. The largest change in relative variability is seen for large plankton biomass between 60N and 80N (dashed lines),

which increases from 10-12% in the annual mean to the ~50% seasonally in the CORE model and 75-80% seasonally in ESM2.1. By contrast, the relative variability goes from about 30% in the annual mean to about 40% for April alone for large plankton in the tropics, a much smaller increase. Relative variability remains relatively small throughout the Southern Hemisphere. Roughly the opposite geographic pattern is seen in the austral spring (October, Figure 4d), with the Southern Hemisphere showing a large increase south of 60S, with average relative variability in large biomass reaching 70% at some latitudes. Again we see that the CORE forced model tends to have less variability than ESM2.1 at high latitudes and a little more variability in the tropics. The month of July (Figure 4c) looks more like the interannual variability, with a tropical peak and lower values in the high latitudes. The actual values are higher, as the mean relative variability from 30S to 30N is 35% in ESM2.1 during July vs. 24% in the annually-smoothed version, but this is a much smaller increase than that seen at high latitudes. The picture that emerges then is one where changes in bloom timing dominate variability at high latitudes, and changes in both timing and magnitude are important at low latitudes.

As shown in Figure 5, the basic spatial pattern of interannual variability in the springtime large phytoplankton biomass resembles that seen in the chlorophyll, but with a much greater range. As in the SeaWiFS annual data, regions of high variability are seen at the boundary between the subtropical gyre and the high-nutrient equatorial zone, but also in mode water formation regions where deep mixed layers are found along the boundary of the subtropical and subpolar gyres. High variability is also found in convective regions within the subpolar Weddell Sea, Bering Sea, and North Atlantic.The difference between the left and right-hand columns of Figure 5 reinforces the result from Figures 3 and 4 that chlorophyll or total biomass alone can give an inaccurate picture of the interannual variability within an ecosystem.

The three key results of this section are thus that large plankton vary more than small plankton, that large relatively variability is found on the edges of highly productive regions, and that relative variability during the spring bloom is larger than variability over the entire year. The following section expands upon the second of these results, looking at the boundary between the equatorial upwelling and subtropical gyre, showing that the changes in concentration are associated with changes in the areal extent of the oligotrophic gyre, and considering the physical forcing driving such changes. Section 5 examines mechanisms behind springtime variation in large phytoplankton concentrations in four regions: the subtropical gyre off Hawaii, the Kuroshio extension, the Sea of Okhotsk and the Western Bering Sea

4. Interannual changes in biome area: The case of the equatorial upwelling

We begin with the equatorial Pacific where interannual variability is high and breaking down this variation month by month yields less of an increase (Fig. 3) than in high latitudes. The variability in this region is relatively consistent between the CORE and ESM2.1 runs, with both models simulating the largest variability around the edge of the high-nutrient cold tongue- a picture similar to that seen in Figure 1c. If we define the boundary between the equatorial upwelling biome and oligotrophic gyre/subtropical biome either by using the chl=0.07 mg/m^3 isoline (following Polovina et al., 2008) or the NO_3=0.02 mmol/m^3 line (Figure 6a) between 20S and 20N, we see that the CORE model shows the gyres expanding and contracting with decadal and interannual frequencies. Although nitrate is only one of the sources of nitrogen for the off-equatorial regions in this model, it is used as an indicator of upwelled nutrient. The changes in oligotrophic gyre area can be regressed onto changes in chlorophyll (colors, Fig. 6b) showing

that a larger oligotrophic gyre area is associated with lower chlorophyll concentrations at the edge of the high nutrient waters. Regressing gyre area onto wind stresses (vectors, Figure 6b), shows that higher oligotrophic gyre areas are associated with anomalous easterlies along the gyre margins. The correlation between equatorial winds and tropical oligotrophic gyre area over this time period is 0.77, while off-equator, the correlations approach 0.85.

We examine the mechanistic connection between winds, currents and the area of the subtropical biome by looking at the mass balance of nitrogen in the CORE runs in three areas outlined by the green lines in Figure 7b. Changes in nitrate import that explain a large fraction of changes in the vertical particle export flux can be identified as important causative agents for export flux variability. Which fluxes are the most important end up being slightly different for the regions on and off the equator. Along the equator (175E-160W, 3S-3N) the anomalous advection of nitrate from below and from the east together (red line, Fig. 7a) correlate well with the particle export anomaly at 100m (black line Fig. 7a). However, this correlation is not simply due to the direct response of wind-driven currents acting on the background nutrient field. The flux due to changes in currents alone (blue line, Fig. 7a) has a strikingly lower correlation with the particle export (0.36 vs. 0.9) and a lower amplitude of variability. In the northern center of action (165W-140W, 5N-15N) the dominant control of the particle export is from advection of nutrient into the region from the south (compare black and red lines, Fig. 7b). Here too, however, changes in the velocity alone account for only a small part of the variability, implying that changes in the nutrient concentrations of the inflow are dominant. The dominance both of north-south advection and of changes in nutrient concentrations in explaining such changes in advective flux is also found in the region from 140W-100W, 8S-15S (Figure 7c). This region covers the southern center of action in Figure 6b (while the blue and black lines do not in fact

look well correlated, they in fact match up extremely well until the 1980s). In all three regions, the changes in export represent changes in the regional extent of the highly productive, nutrient rich waters, not just local changes in productivity. This implies that predicting the change in biome area involves more than just predicting changes in the amplitude of ENSO- one must also understand the changes in the background field of nutrients.

5. Variability of large phytoplankton biomass in the North Pacific during boreal spring

a.) Identification of different regimes

Turning to variability in the timing of the spring bloom, we see that the relationship between local sea surface temperature and biological cycling during April shows a complicated pattern in the North Pacific (Figure 8). Both chlorophyll and large plankton biomass show a rough consistency, with a tongue of high variability negatively correlated with SST extending from the center of the subtropical gyre to the northeast off the Pacific coast of Canada, weak positive correlation in the northwest Pacific, stronger positive correlation Sea of Okhotsk and a region of strong negative correlation in the western Bering Sea off of Kamchatka. The variation of large biomass and chlorophyll are only of similar magnitude in the first of these regions. In the region from 150E-160E and 36N-40N (in the Kuroshio extension) chlorophyll shows a relative variability of 35% as opposed to 98% for large phytoplankton biomass and similar differences are found in the Sea of Okhotsk and Western Bering Sea. However, as shown in the following sections, the physical mechanisms underlying this variability differ in each of the regimes denoted by the green boxes in Figure 8.

b.) The subtropical gyre

In the subtropical gyres, downwelling and high vertical gradients in temperature combine to create regions with low surface nutrients. Although sometimes referred to as biological deserts, these regions do support some pelagic fisheries. In such nutrient-limited low-latitude regimes one would expect surface cooling to lead to more mixing, more nutrient supply and thus higher productivity. Thus mixed layer depth would be expected to be positively correlated with biomass and chlorophyll in tropical and subtropical regions. Follows and Dutkewicz (2002) compared a model forced in a similar manner to ours with SeaWiFS chlorophyll in the subtropics. Comparing modeled mixed layer depth and observed chlorophyll, their work supported the idea that the increased chlorophyll was associated with increased vertical supply of nutrients.

Does this mechanism carry over to the spring bloom in the month of April? Examination of a region of the subtropical North Pacific near Hawaii, from 170W-160W and 26-30N shows a basic consistency with the classic picture, but with some complications (Figure 9a). The linkage between high nitrate, low SSTs and enhanced biomass does hold, not only during the month of April but three months earlier during January. However, the linkage with mixed layer depth is more complicated, as high biomass in April is better correlated with deeper mixed layers during the winter (consistent with more wintertime mixing of nutrients) but also with shallower mixed layers and more mixed layer light in April. The negative correlation with iron shows that iron cannot be is the dominant limiting nutrient (this is in general the case away from the center of the Peru upwelling and the Southern Ocean). It is worth noting that the correlation between April large biomass and January mixed layer depth is smaller in magnitude than the anticorrelation

with temperature- suggesting that some of the variability in nutrient may result from southward advection of colder, fresher northern waters.

c.) The Kuroshio extension- a mode water formation region

Moving further to the north, we come to a region that has a strong seasonal cycle in mixed layer depth at the edge of the subtropical gyre. Deeper wintertime mixing means that springtime light limitation can be more extreme in this region, which is associated with formation of key mode waters. Nutrients in the Kuroshio extension are more abundant than in the subtropical gyre, though at lower levels than in the subpolar gyre, with the result that chlorophyll levels are somewhat lower than in the subpolar gyre. Sarmiento et al. (2004) defined this region as a combination between the subtropical seasonal stratified biome and subpolar gyre biome, while Polovina et al. (this volume) include it in the temperate biome. As shown in Figures 8b and 9b, the large interannual variability in April large phytoplankton biomass in this region is only weakly correlated with temperature, but is very strongly *anticorrelated* with mixed layer depth and positively correlated with mixed layer light availability. Light limitation, rather than nutrient limitation plays a dominant role here so that the springtime shallowing of the mixed layer triggers a bloom. Such shallowing can result either from local warming or from the advection of fresher, colder waters from the north, hence the lower correlation with sea surface temperature. In contrast to the center of the subtropical gyre, there is relatively little correlation with conditions in January, suggesting that this will be a challenging region to predict.

d.) The Sea of Okhotsk- A marginal ice zone biome

A third region outlined in Figure 8 is the Sea of Okhotsk, which is ice covered during the wintertime and as such was classified by Sarmiento et al. (2004) as part of the marginal ice zone biome. Interannual variability of large phytoplankton biomass in this region is strongly correlated with temperature and light availability, but only weakly anticorrelated with mixed layer depth (Figure 9c). The correlation between April large phytoplankton biomass and sea ice concentration is -0.72, comparable to the 0.86 correlation with mixed layer light. This is consistent with variability in the timing of ice breakup being important for allowing relief of light limitation and drawdown of surface nutrient, but with also with higher temperature being associated with shallower surface mixed layers.

The correlation between mixed layer light and chlorophyll (0.50, not shown) is much lower than the correlation between mixed layer light and both large and small phytoplankton biomass (0.86). This reflects the fact, previously noted, that the phytoplankton in the TOPAZ model adapt to light availability, reducing their chlorophyll to carbon ratio as more light becomes available. As a result, the chlorophyll to carbon ratio in the Sea of Okhotsk during the month of April is strongly anticorrelated with mixed layer light (-0.63) reducing the amplitude of chlorophyll variability and showing again why it is necessary to be cautious in extrapolating from satellite chlorophyll to ecosystem state.

e.) The Western Bering Sea- A salinity stratified subpolar biome

A final region of interest is found in the western Bering Sea, where there is large interannual variability in large phytoplankton biomass but an anticorrelation with temperature. As shown in Figure 9d, this region is also light limited, and large phytoplankton biomass is strongly anticorrelated with mixed layer depth. The anticorrelation with temperature, which stands in contrast to the Kuroshio extension and Sea of Okhotsk means that salinity, rather than temperature is the dominant mechanism establishing mixed layer stratification in this region. This dynamical regime is also found in many other parts of the model ocean, including the southern Labrador Sea, central Norwegian Sea and Weddell Sea.

The mechanisms by which such salinity anomalies develop are potentially complicated. Gargett (1997) looked at salmon stocks in the North Pacific and argued that the key variable for explaining coastal stability was Alaskan streamflow, which freshened coastal regions and was tied to the changes in low pressure associated with the PDO. However other analysis we have done of the CM2.1 model (Gnanadesikan et al., Variability of ventilation in the North Pacific in a coupled model, in prep.) in the western Bering Sea suggests that here the dominant driver of salinity variability is not the supply of fresh water, but rather the upwelling of salty deep water from below as a result of local changes in the wind stress curl. Galbraith et al. (subm.) look at similar salinity anomalies in a coarse-resolution coupled model in the Southern Ocean, and find that the source of the anomalies is a combination of precipitation anomalies and entrainment of saltier deep waters.

6. Discussion and conclusions

The coupled physical-biogeochemical models used to assess climate change impacts on ocean ecosystem offer insights as to how changing prey availability for fisheries may be linked to climate. We review these insights below, and consider the potential implications for predicting and diagnosing marine ecosystem variability.

a.) The importance of size structure

The first major message of this paper is that one should not expect a straightforward scaling between primary productivity or chlorophyll and the biomass of the large phytoplankton that are thought to be most important for fisheries. Over much of the ocean, large plankton appear to respond disproportionately to changes in environmental conditions, driven by differential uptake of nutrients and a size-dependent grazing parameterization (Fig 2d, 3-5,8). Because photoadaptation causes the chl:C ratio to drop as more light becomes available, regions which are light limited show much less variability in chlorophyll than in large plankton biomass. This suggests that in order to track prey availability, fisheries oceanographers need to look to satellite estimates of phytoplankton carbon biomass (such as that proposed by Behrenfeld et al. 2005) as well as those that separate out phytoplankton into different size classes (Kostadinov et al., 2009, Mouw et al. , subm). Although these products remain preliminary, the fisheries oceanography community should consider using them, especially where results from chlorophyll or primary productivity seem to contradict inferences made from looking at fisheries data. Additionally, when examining simulations from earth system models, fisheries oceanographers should be careful to focus on the fraction of productivity associated with large phytoplankton,

and not simply assume that the total primary productivity or chlorophyll concentration will tell the whole story.

b.) The potential importance of timing

The second key message of this paper is that models show much more variation in the interannual variability of phytoplankton biomass associated with the spring bloom than in the interannual variability in annually averaged phytoplankton biomass. For high latitude regions and also when large phytoplankton are considered in isolation the difference can approach an order of magnitude-supporting the Hjort-Cushing "match-mismatch" hypothesis. Larger variability in bloom timing relative to interannually integrated production has been seen in individual ecosystems (e.g. Hunt et al., 2002; Henson and Thomas, 2005), but this study breaks new ground in looking at the global distribution of relative interannual variability in large phytoplankton biomass during the spring. Variability in bloom timing has potentially important implications for fisheries oceanographers using models such as Ecopath, which often either use annual integrated primary productivity (Guennette et al., 2006; Howell et al., 2010) or diagnose this quantity from lower trophic level biomass (Piroddi et al., 2010). Our results suggest that such models may need to take bloom timing into account if they are to properly estimate the range of climate-forced ecosystem variability.

Bloom timing may be particularly important for understanding different climate reponses between "capital breeders" which build up a large stock of resources before breeding, and "income breeders" which match food and breeding (Jonsson, 1997). For example, Boulcott and Wright (2008) argue that variability in the timing of blooms in the North Sea has a particularly

strong impact on the regional distribution of sandeels. Insofar as income breeders average over the entire seasonal cycle, by contrast, they may be less vulnerable to such variability, as noted by Martin and Wiebe (2004) for arctic and alpine birds and Takasuka et al. (2010) for Japanese anchovy as opposed to Japanese sardine. Understanding such tradeoffs may be a fruitful area of collaboration between biogeochemical modelers and fisheries oceanographers.

c.) Changes in tropical biome extent: implications for predictability

Both observations (Fig 1) and models (Fig 3, 5) show the large relative variability on the edges rather than in the centers of highly productive regions. This may be important, as many organisms have planktonic larval stages, and many of the highly productive regions (in particular coastal and equatorial upwelling zones) are divergent. Larvae spawned in such regions may thus be carried out of them on time scales of a few weeks, and whether they are able to return may depend more on the food they find on the edges of the unproductive gyres than in the center of the upwelling regions. We suggest more study of whether larval survival within these edge regions is important for certain species. Additionally, the edges of high productivity regions may be more favorable for visual predators such as tuna, which may trade off the requirement for relatively clear water in order to detect and capture prey with higher prey densities in more turbid waters (Kirby et al., 2000).

Variations in the edges of the gyres have been linked to climate change by Polovina et al. (2008) who saw an increase in the area of the oligotrophic gyres during the SeaWiFS era. However, when Henson et al. (2010) compared historical trends in gyre area with several CORE-forced ocean biogeochemistry models (including the one used here) they found a generally good

agreement between modeled and observed gyre size (0.88 for the SeaWiFS era) but also found that the variability during the SeaWiFS era was much smaller than that required to detect an anthropogenic signal. Given the deficiencies of an Eulerian interpretation of ocean biome variability on short time scales (Figure 7) as well as previous results indicating that there are changes in the large-scale ventilation structure of the ocean under global warming (Gnanadesikan et al., 2007), it will be essential not to depend on physical models alone to predict the behavior of these biome boundaries.

d.) Challenges in modeling high latitude variability

We have shown that interannual variation in the monthly distribution of productivity may be much larger than the interannual variation in the mean productivity (Fig. 4,5) and that in high latitudes salinity can play an important role in explaining this variability (Fig. 9). Variability in salinity presents a challenge to retrospective analyses of ecosystem variability. As seen in Figures 4 and 5 the high latitude variation in springtime production is higher in ESM2.1 coupled climate models than in the CORE ocean-only reanalysis model. A primary reason for this is that ocean-only models run with "observed" precipitation must be also run with a flux correction by which salinities are restored to their climatological values. Without such a restoring, a chain of feedbacks may be triggered at high latitudes whereby cooling in convective regions leads to precipitation exceeding evaporation, resulting in a buildup of freshwater at the surface, suppression of convection, and further cooling. In the real world, cooling a drop in surface temperatures would also be expected to lead to a decrease in precipitation, but this feedback is absent in CORE-forced runs. However the presence of restoring can damp interannual variability

in salinity, especially when it is associated with large-scale advection of surface anomalies. The challenge then is for the climate community to develop methods of reanalysis that can properly simulate the variability in winds and heating without damping out hydrological feedbacks. Coupled reanalyses (Zhang et al., 2007) in which the atmospheric winds are nudged towards observed values may provide such consistent solution, but ecosystem models have yet to be included in these systems. In the interim, fisheries oceanographers using CORE-forced runs need to carefully evaluate whether observed salinity variability is properly captured.

Acknowledgments: Rob Armstrong and Jorge Sarmiento helped formulate our original implementation of size structure within the models. Charlie Stock and Ryan Rykaczewski have helped us understand the implications and limitations of this approach and provided useful reviews of this manuscript. Thanks to Jon Hare for useful discussions and for the invitation to give this talk at the Sendai Meeting.

References

Agawin, N. S. R., Duarte, C.M, and Agusti,S. 2000. Nutrient and temperature control of the contribution of picoplankton to phytoplankton biomass and production, Limnology and Oceanogrraphy, 45: 591– 600.

Aumont, O., and Bopp, L. 2006. Globalizing results from ocean in situ iron fertilization studies: Global Biogeochemical Cycles, 20: GB2017 doi:10.1029/2005GB002591.

Behrenfeld, M.J., Boss, E., Siegel, D.A. and Shea, D.M. 2005. Carbon-based ocean productivity and phytoplankton physiology from space, Global Biogeochemical Cycles, 19, GB1006, doi:10.1029/2004GB002299.

Bigelow, H.B. 1926. Plankton of the offshore waters of the Gulf of Maine, Bulletin US Bureau of Fisheries, 40, 509pp.

Boulcott, P and Wright. P.J. 2008. Critical timing for reproductive allocation in a capital breeder: evidence from sandeels, Aquatic Biology, 3, 31-40.

Carr, M.-E. 2002. Estimation of potential productivity in Eastern Boundary Currents using remote sensing, Deep Sea Research, Part II, 49: 59–80.

Chavez, F.P., Ryan, J., Lluch-Costa, S.E. and Niquen M. 2003. From anchovies to sardines and back, multidecadal change in the Pacific Ocean, Science, 299, 217-221.

Cushing, D.H. 1990. Plankton production and year-class strength in fish populations: an update of the Match/Mismatch hypothesis, Advances in Marine Biology, 26, 249-293.

Delworth, T.L. and co-authors 2006. GFDL's CM2 global coupled climate models: Part 1-Formulation and simulation characteristics, Journal of Climate, 19: 643-674.

Dugdale, R.C. and Goering, J.J. 1967. Uptake of new and regenerated forms of nitrogen in primary productivity, Limnology and Oceanography, 12: 196-206.

Dunne, J.P., Armstrong, R.A., Gnanadesikan,A. and Sarmiento, J.L. 2005. Empirical and mechanistic models of the particle export ratio, Global Biogeochemical Cycles, 19: GB4026, doi:10.1029/2004GB002390.

Dunne, J. P., Sarmiento, J.L., and Gnanadesikan,A. 2007. A synthesis of global particle export from the surface ocean and cycling through the ocean interior and on the seafloor. Global Biogeochemical Cycles, 21: GB4006, doi:10.1029/2006GB002907.

Dunne, J.P., Galbraith, E.D., Gnanadesikan,A., John, J., Sarmiento, J.L., Slater, R.D., and Griffies, S.M. 2010. Implications of elemental coupling in a global ocean biogeochemistry/general circulation model, in prep. for Biogeosciences

Follows, M. and Dutkewicz, S. 2002. Meteorological modulation of the North Atlantic Spring Bloom, Deep Sea Research Part II, 49: 321-344.

Galbraith, E.D., Gnanadesikan, A., Dunne, J.P. and Hiscock, M.R. 2010. Regional impacts of iron-light co-limitation in a global biogeochemical model, Biogeosciences, 7: 1043-1064.

Gargett, A.E. 1997. The optimal stability “window”: a mechanism underlying decadal fluctuations in North Pacific salmon stocks? Fisheries Oceanography, 5, 109-117.

Genner, M.J., Sims, D.W., Wearmouth, V.J., Southall, E.J., Southward, A.J., Henderson, P.A. and Hawkins, S.J. 2004, Regional climatic warming drives long-term community changes of British marine fish, Proceedings of the Royal Society B, 655-661.

Glynn, P.W. and deWeerdt, W.H. 1991.Elimination of two reef-building hydrocorals following the 1982-1983 El Nino warming event, Science, 253, 69-71.

Gnanadesikan A., and co-authors, 2006. GFDL’s CM2 Global Coupled Climate Models- Part 2: The baseline ocean simulation, Journal of Climate, 19, 675-697.

Gnanadesikan, A., Russell, J.L. and Zeng, F. 2007. How does ocean ventilation change under global warming? Ocean Science,3, 43-53.

Griffies, S.M. and co-authors, 2009. Coordinated Ocean-ice Reference Experiments (COREs), Ocean Modelling, 26: 1-46.

Griffies, S.M. Gnanadesikan, A., Dixon, K.W., Dunne, J.P., Gerdes, R.. Harrison, M.J., Rosati, A., Russell, J. L., Samuels, B. L., Spelman, M.J., Winton, M. and Zhang, R. 2005. Formulation of an ocean model for global climate simulations. Ocean Science, 1: 45-79.

Guenette, S., Heymans, S.J.J., Christensen, V. and Trites, A.W., Ecosystem models show combined effects of fishing, predation, competition and ocean productivity on Steller sea lions, (Eumetopas jubatus) in Alaska, Canadian Journal of Fisheries and Aquatic Sciences, 63, 2495-2517, 2006.

Henson, S.A., Sarmiento, J.L., Dunne, J.P, Bopp, L., Lima, I., Doney, S.C., John, J. and Beaulieu, C. 2010. Detection of anthropogenic climate change in satellite records of ocean chlorophyll and productivity, Biogeosciences, 7, 621-640.

Henson, S. and Thomas, A. 2007. Interannnual variability in timing of bloom initiation in the California Current System, Journal of Geophysical Research Oceans, 112, C08007, doi:10.1029/2006JC003960.

Hjort, J. 1914. Fluctuations in the great fisheries of northern Europe viewed in the light of biological research. Rapp. Cons. Explor. Mer., 20:1-228.

Howell, E.A., Dunne, J.P. and Polovina, J.J. 2010. Modelling the central North Pacific ecosystem response to predicted climate variations and fishery management scenarios, Climate Change Effects on Fish and Fisheries, Sendai, Japan, 139.

Hunt, G.L., Stabeno, P., Walters, G., Sinclair, E., Brodeur, R., Napp, J.M. and Bond, N.A., 2002. Climate change and control of the southeastern Bering Sea pelagic ecosystem, Deep Sea Res. II, 49, 5821-5853.

Jonsson, K.I. 1997. Capital and income breeding as alternative tactics of resource use in reproduction, Oikos, 78, 57-66.

Klausmeier, C., E. Litchman, Daufresne, T. and Levin, S.A., 2004. Optimal nitrogen-to-phosphorus stoichiometry of phytoplankton, Nature, 429, 171-174.

Kirby, D.S., Fiksen, O., Hart, D.J.B. 2000. A dynamic optimisation model for the behaviour of tunas at ocean fronts, Fisheries Oceanography, 9, 328-342.

Kostadinov, T.S., Siegel, D.A., and Maritorena, S. 2009. Retrieval of the particle size distribution from satellite ocean color observations. Journal of Geophysical Research – Oceans, 114: C09015, doi:10.1029/2009JC005303.

Mantua, N.R., Hare, S.R., Zhang, Y., Wallace, J.M. and Francis, R.C. 1997. A Pacific interdecadal climate oscillation with impacts on salmon production, Bulletin of the American Meteorological Society, 78: 1069-1079.

Martin, K. and Wiebe, K.L. 2004. Coping mechanisms of alpine and arctic breeding birds: Extreme weather and limitations to reproductive resilience, Integrative and Comparative Biology, 44, 177-185.

Martinez, E., Antoine, D., D'Ortenzio, F. and Gentili, B. 2009. Climate-driven basin-scale decadal oscillations of oceanic phytoplankton, Science: 326, 1253-1256.

Moore, J.K., Doney, S.C., Kleypas, J.A., Glover, D.M., and Fung, I.Y. 2002. An intermediate complexity marine ecosystem model for the global domain: Deep-Sea Research II, 49: 463-507.

Platt, T., Subba Rao, D.V. and Irwin, B., 1983. Photosynthesis of picoplankton in the oligotrophic ocean, Nature, 301, 702-704.

Polovina, J.J., Howell, E.A. and Abecassis, M. 2008. Ocean's least productive waters are expanding, Geophysical Research Letters, 35, L03618, doi:10.1029/2007GL031745.

Reichler, T. and Kim, J. 2008. How well do coupled climate models simulate today's climate?, Bulletin of the American Meteorological Society, 89: 303–311.

Russell, J.L., Stouffer, R.J. and Dixon, K.W. 2006. Intercomparison of the Southern Ocean Circulations in IPCC Coupled Model Control Simulations. Journal of Climate, 19(18): 4560-4575, doi:10.1175/JCLI3869.1.

Ryther, J.H. 1969. Photosynthesis and fish production in the sea, Science, 166, 72-76.

Six, K.D. and Meier-Reimer E. 1996. Effects of plankton dynamics on seasonal carbon fluxes in an ocean general circulation model, Global Biogeochemical Cycles, 10, 559-583.

Steinacher, M., Joos, F., Frohlicher, T, and coauthors 2010. Projected 21st century decrease in marine productivity: a multi-model analysis, Biogeosciences, 7, 979-1005, doi:10.5194/bg-7-979-2010.

Sugimoto, T., Kimura, S. and Tadokoro, K. 2001. Impact of El Nino events and climate regime shift on living resources in the western North Pacific, Progress in Oceanography, 49, 113-127.

Takasuka, A., McClatchie, S., Weber, E., Oozeki, Y., Kameda, T., Hirota, Y. and Okamura, H. 2010. Responses of anchovy and sardine spawning to physical and biological factors in the Kuroshio and California Current systems: Interspecific and intersystem comparison, in Climate Change Effects on Fish and Fisheries, Sendai Japan, 107.

van Oldenborgh, G. J., Philip, S. Y., and Collins, M. 2005. El Nino in a changing climate: a multi-model study, Ocean Science, 1: 81–95.

Wittenberg, A. T., Rosati, A., Lau, N. G., and Ploshay, J. J. 2006. GFDL's CM2 Global coupled climate models, Part III: Tropical Pacific Climate and ENSO, J. Climate, 19, 698–722.

Zhang, S., Harrison, M.J., Rosati, A. and Wittenberg, A.T., 2007. System System Design and Evaluation of Coupled Ensemble Data Assimilation for Global Oceanic Climate Studies. Monthly Weather Review, 135(10), 3541-3564, doi:10.1175/MWR3466.1.

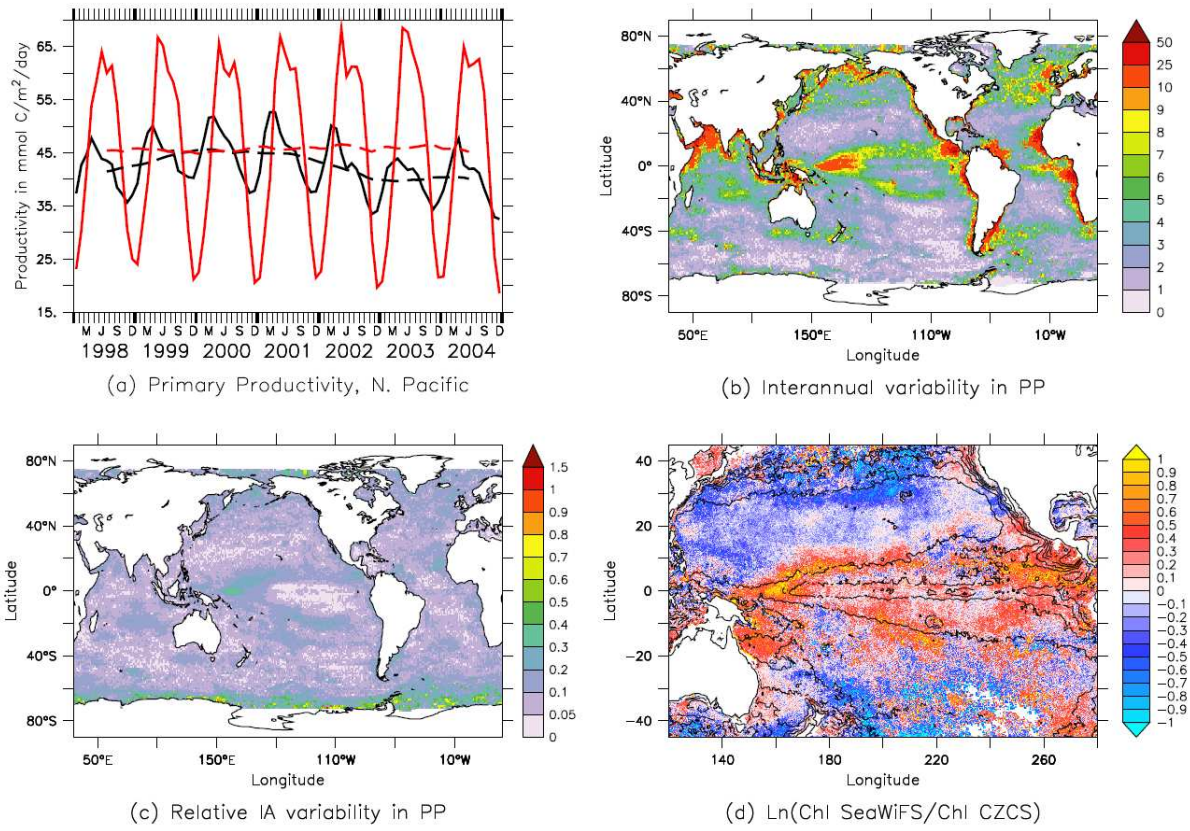

Figure 1: (a) Variability in phytoplankton productivity inferred from the SeaWiFS satellite using the Carr (2002) algorithm. Red lines show latitudes 30N-60N, black lines latitudes 0-30N. Dashed lines show 12 month smooth. (b) Interannual variability in SeaWiFS productivity (standard deviation of productivity) using same data as in (a). (c) Relative interannual variability (normalized by the mean value) (d) Natural log of the change in chlorophyll between the SeaWiFS and CZCS eras after Martinez et al. (2009) data courtesy of Elodie Martinez. Contours show mean chlorophyll concentration with a contour interval of 0.1 mg/m^3. Note that much of the variability is on the edge of regions with higher chlorophyll.

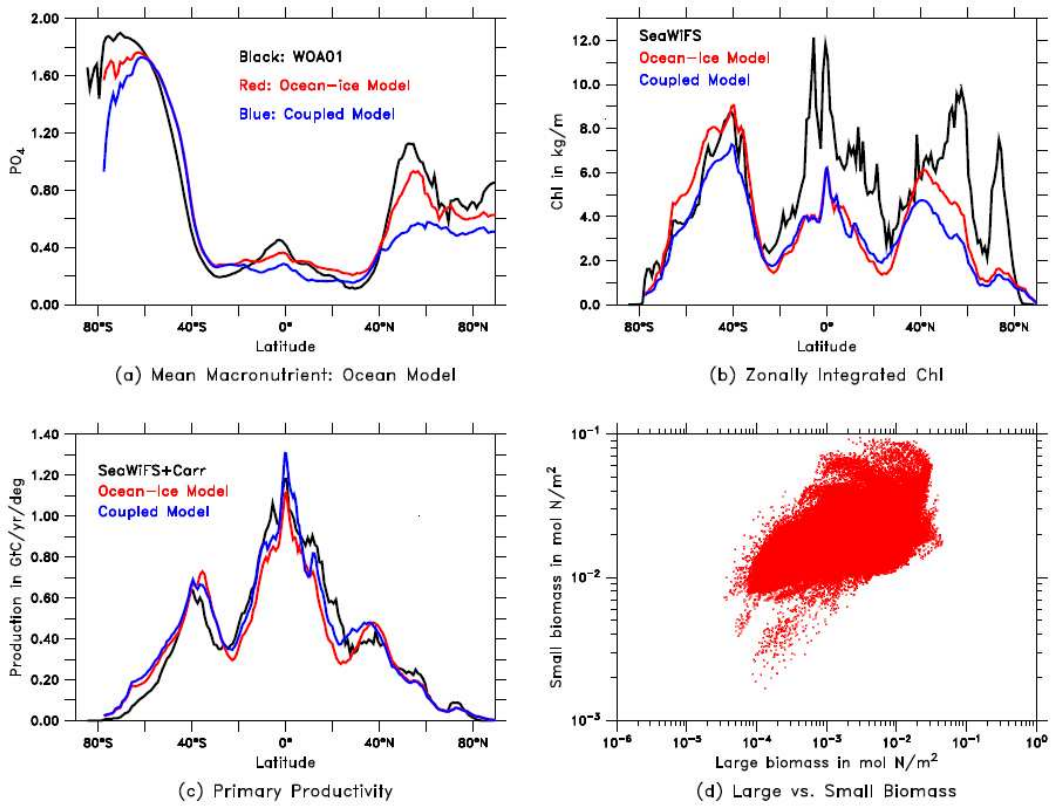

Figure 2: Evaluation of model fidelity. (a) Annual mean surface phosphate from data (WOA01, Conkright et al., 2002), the ocean-ice model (red) and the coupled earth system model (blue). (b) Zonally integrated chlorophyll the SeaWiFS satellite (black) compared with surface chlorophyll from the models. (c) Primary productivity compared with that estimated from the SeaWiFS satellite using the algorithm of Carr (2002). (d) Size structure in the ocean-only model. Horizontal axis is large nitrogen biomass, vertical axis is small nitrogen biomass. Only output from 60S-60N is considered to avoid months with total darkness.

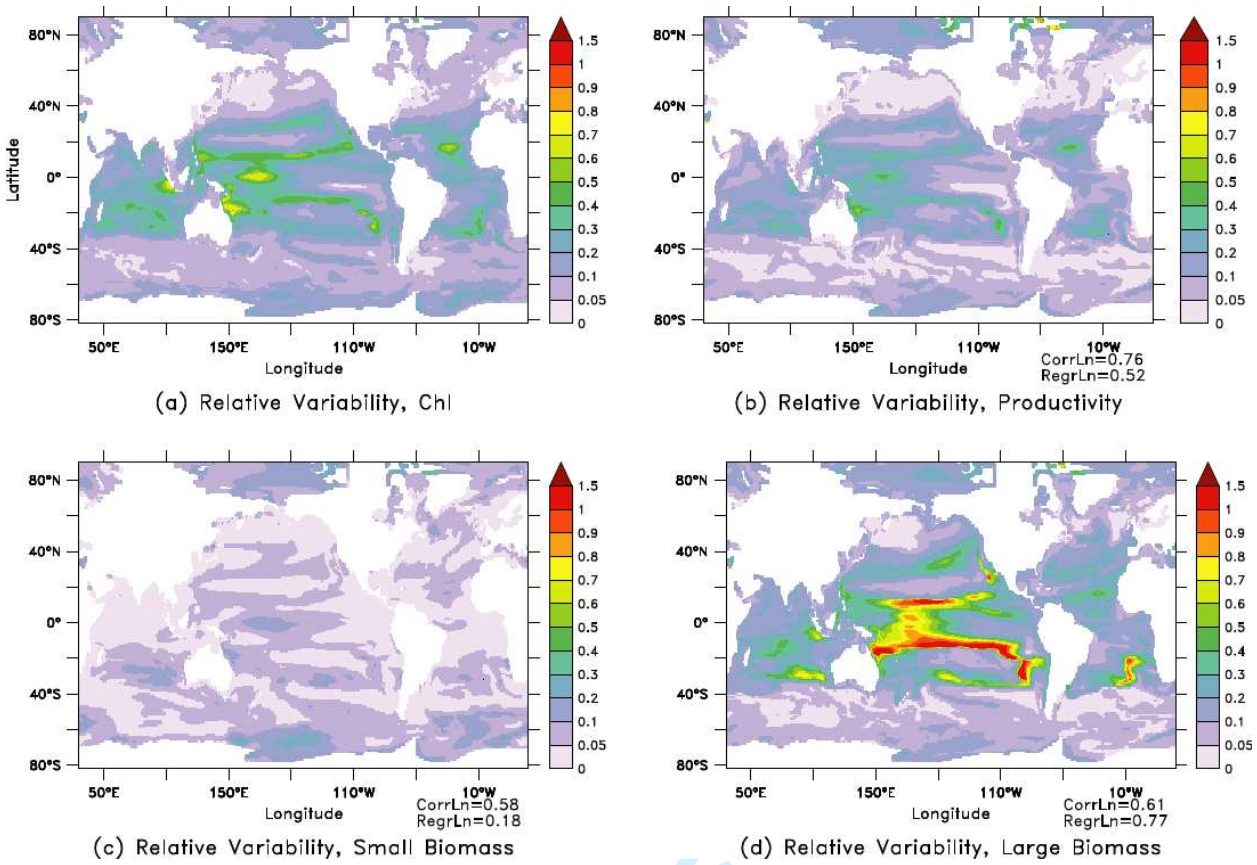

Figure 3: Simulated historical relative interannual variability (standard deviation/mean) in a number of quantities in a CORE-forced (Griffies et al. 2009) ocean-ice model. Correlations and regressions between the natural log of chlorophyll and the natural log of the relevant quantity are shown to give a sense of power law relationships. (a) Surface chlorophyll. (b) Productivity (total grazing 0-100m). (c) Small biomass 0-100m. (d) Large biomass 0-100m.

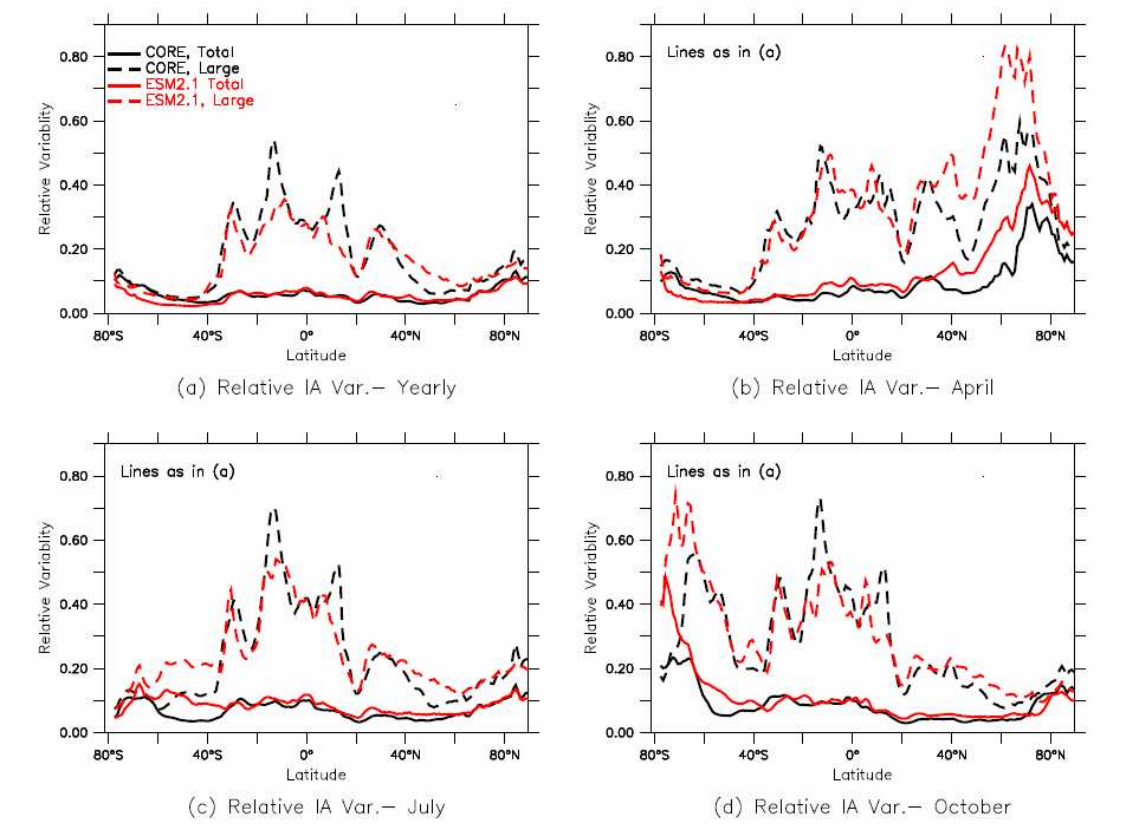

Figure 4: Zonally averaged relative standard deviation of phytoplankton biomass (standard deviation/mean) as a function of space and time. Red lines are for years 401-500 of ESM2.1, black lines for the CORE forced run. Solid lines are for total phytoplankton biomass, while dotted lines are for large phytoplankton biomass alone. (a) Variability of 12-month smoothed biomass. (b) Same as (a) but only for the month of April. (c) Same as (a) but only for the month of July. (d) Same as (a) but only for the month of October.

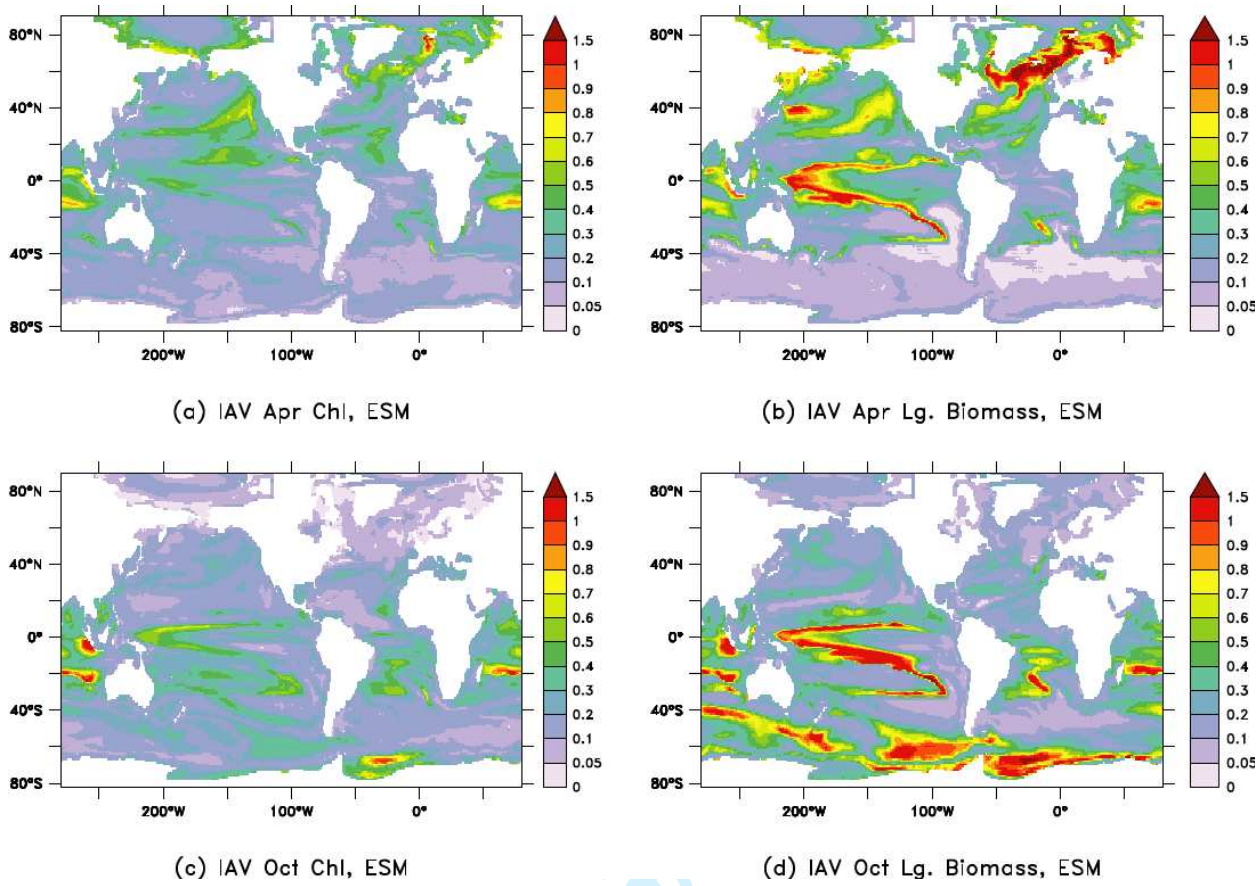

Figure 5: Interannual variability in spring/fall for the Earth System model. All plots show standard deviation over mean. (a) Surface chlorophyll, April. (b) Large phytoplankton biomass, April. (c) Surface chlorophyll, October. (d) Large phytoplankton biomass, October.

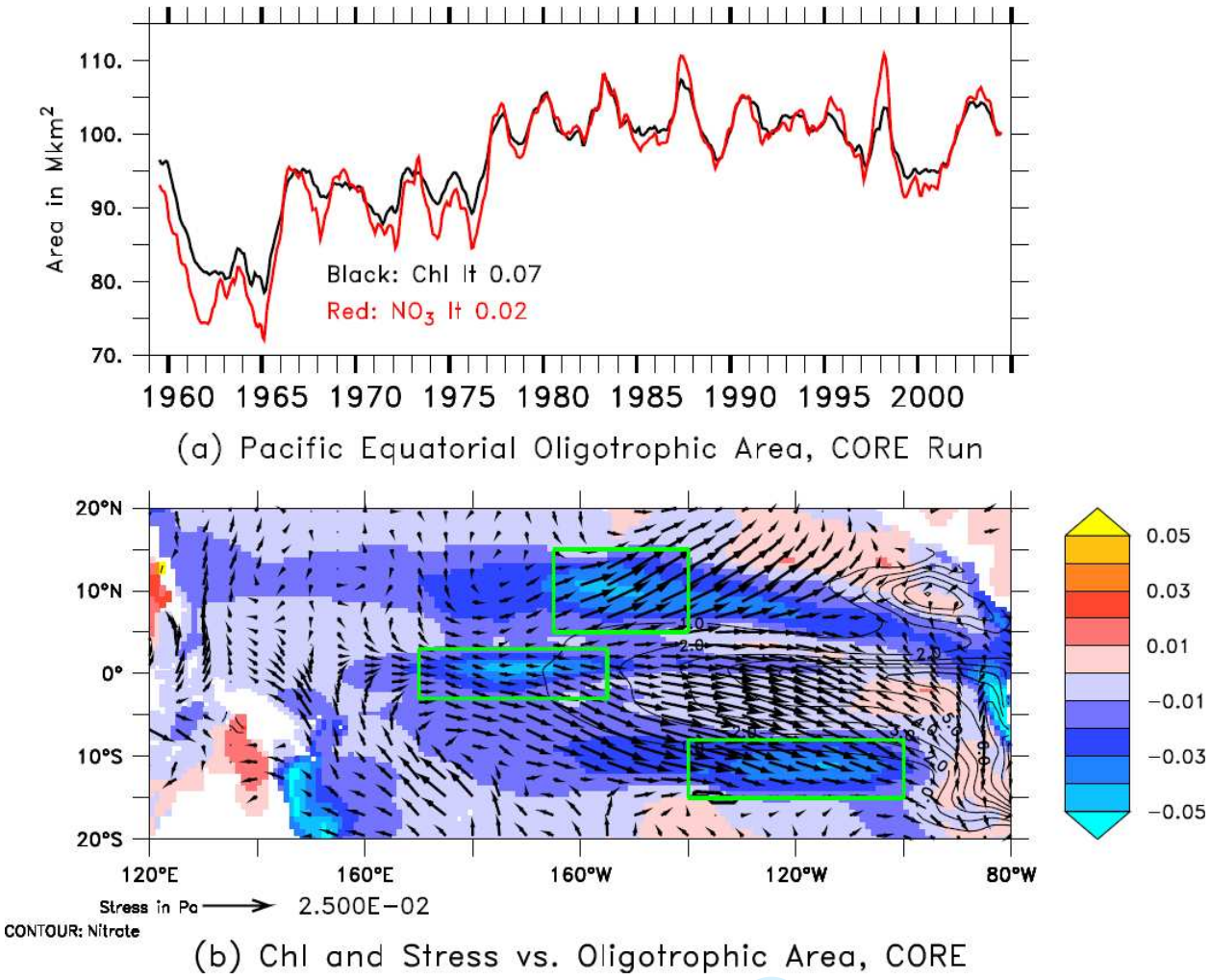

Figure 6: Changes in oligotrophic gyre area in the Central Pacific (20N-20S, following definition of Polovina et al, 2008). (a) Changes in the oligotrophic gyre area in the CORE forced model. (b) Changes in surface chlorophyll (colors) and on wind stress (vectors) corresponding to a 1 standard deviation change in gyre area.

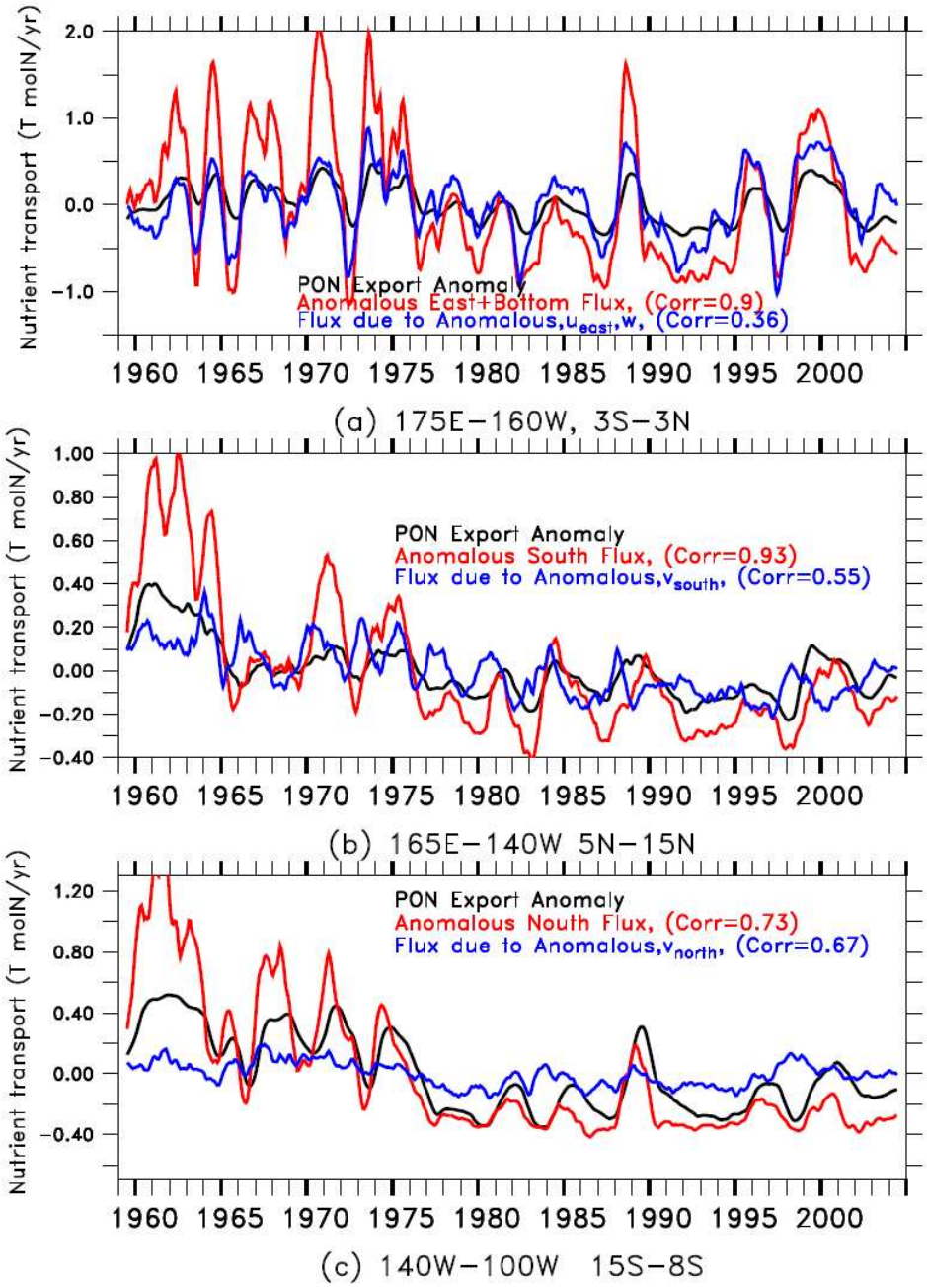

Figure 7: Time series of anomalous export of particulate organic nitrogen (black lines), advective fluxes of nitrate (red lines) and advective fluxes due to changes in velocity alone (blue lines) for the three centers of action in Figure 7. (a) 175E-160W, 3S-3N. (b) 160W-140W, 5N-15N. (c) 140W-100W, 15S-8S.

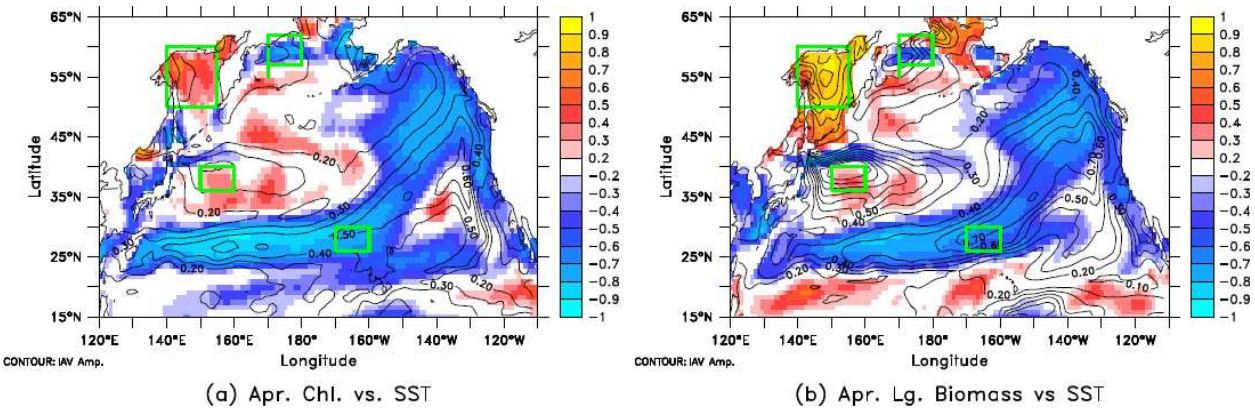

Figure 8: Relationship of variability in local sea surface temperature with variability in (a) chlorophyll and (b) large phytoplankton biomass during the month of April in the North Pacific. Colors show correlation coefficients, contours the interannual variability normalized by the mean as in Figure 5.

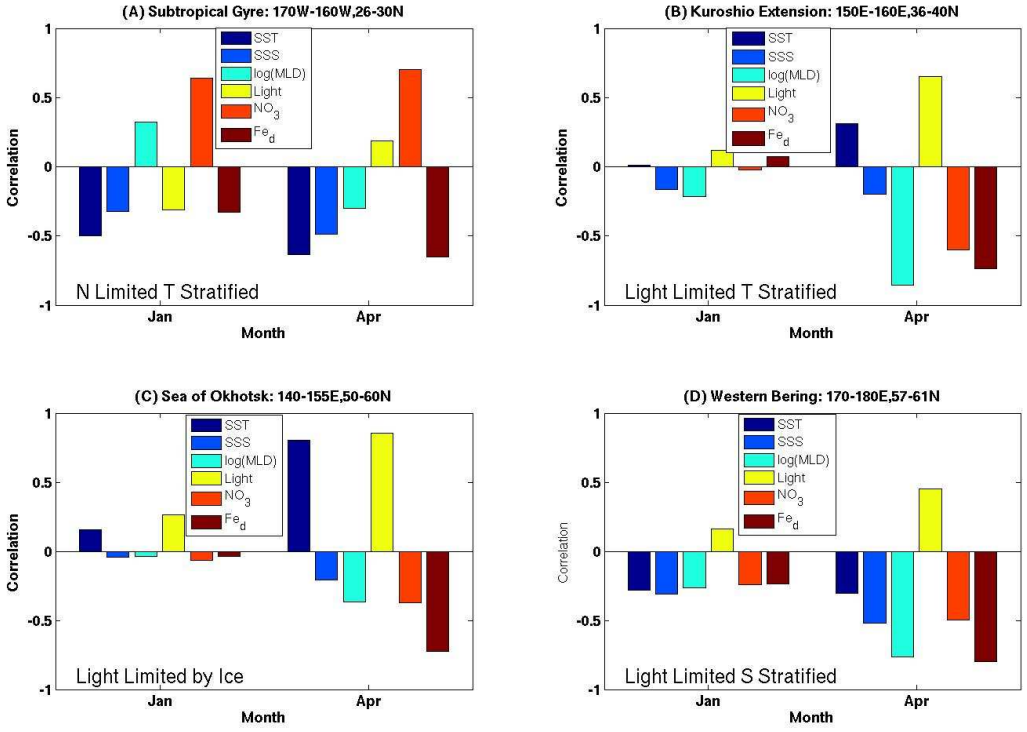

Figure 9: Large phytoplankton biomass during April correlated with other fields at two months (January and April) in the four different dynamical regimes in the North Pacific denoted by the green boxes in Figure 8. (a) Subtropical gyre, 170W-160W, 26N-30N. Dominant correlation is with nitrate both at 0 lag and with a three month lead, consistent with stronger wintertime convection and southward advection of nitrate driving variability. (b) Kuroshio extension region, 150E-160E, 36N-40N. Strong correlation with light, anticorrelation with mixed layer depth at zero lag, little correlation at three month lead, consistent with shallowing of mixed layer playing dominant role. (c) Sea of Okhotsk. Highest correlation at zero lag with nitrate and temperature, consistent with variation in sea ice cover playing dominant role. (d) Western Bering sea. Strong anticorrelation with mixed layer depth, positive correlation with light. Consistent with a light-limited, salinity stratified regime.